BIOCHEMISTRY
including biophysical chemistry & molecular biology
Article

Biochemistry **2010,** *49,* 5321–5330 5321
DOI: 10.1021/bi100434c

The Human HDV-like *CPEB3* Ribozyme Is Intrinsically Fast-Reacting[†]

Durga M. Chadalavada, Elizabeth A. Gratton, and Philip C. Bevilacqua*

Department of Chemistry, The Pennsylvania State University, University Park, Pennsylvania 16802

Received March 23, 2010; Revised Manuscript Received May 25, 2010

ABSTRACT: Self-cleaving RNAs have recently been identified in mammalian genomes. A small ribozyme related in structure to the hepatitis delta virus (HDV) ribozyme occurs in a number of mammals, including chimpanzees and humans, within an intron of the *CPEB3* gene. The catalytic mechanisms for the *CPEB3* and HDV ribozymes appear to be similar, generating cleavage products with 5′-hydroxyl and 2′,3′-cyclic phosphate termini; nonetheless, the cleavage rate reported for the *CPEB3* ribozyme is more than 6000-fold slower than for the fastest HDV ribozyme. Herein, we use full-length RNA and cotranscriptional self-cleavage assays to compare reaction rates among human *CPEB3*, chimp *CPEB3*, and HDV ribozymes. Our data reveal that a single base change of the upstream flanking sequence, which sequesters an intrinsically weak P1.1 pairing in a misfold, increases the rate of the wild-type human *CPEB3* ribozyme by ~250-fold; thus, the human ribozyme is intrinsically fast-reacting. Secondary structure determination and native gel analyses reveal that the cleaved population of the *CPEB3* ribozyme has a single, secondary structure that closely resembles the HDV ribozyme. In contrast, the precleavage population of the *CPEB3* ribozyme appears to have a more diverse secondary structure, possibly reflecting misfolding with the upstream sequence and dynamics intrinsic to the ribozyme. Prior identification of expressed sequence tags (ESTs) in human cells indicated that cleavage activity of the human ribozyme is tissue-specific. It is therefore possible that cellular factors interact with regions upstream of the *CPEB3* ribozyme to unmask its high intrinsic reactivity.

RNA displays a wide variety of functions in biology, including critical roles in cellular catalysis. Naturally occurring ribozymes are widespread, being found in viruses, bacteria, and plants, and include both small and large RNAs, as well as RNP complexes such as the ribosome and spliceosome (*1*−*4*). Self-cleaving RNAs such as hairpin, hammerhead, Varkud satellite, and hepatitis delta virus ribozymes are typically found in viruses, virus satellites, viroids, and satellites of newts, schistosomes, and fungi (*5*−*8*), while the larger Group I and Group II self-splicing RNAs typically occur in fungi, bacteria, and plants (*9*−*11*). HDV[1] was long thought to be the only self-cleaving RNA associated with humans, where it is found within the genome of a pathogen (*12*). Recently, however, two self-cleaving RNAs have been verified in mammals: the CLEC2 ribozyme in the mouse genome (*13*) and the cytoplasmic polyadenylation element-binding protein 3 (*CPEB3*) ribozyme in numerous mammalian genomes, including the human genome (*14*, *15*). In an attempt to understand ribozyme cleavage in the human genome, we focused our studies on the *CPEB3* ribozyme.

An in vitro selection scheme by Salehi-Ashtiani et al. designed to identify ribozymes encoded in the human genome revealed the self-cleaving *CPEB3* ribozyme, which was present within the transcript of a single-copy gene and folded into an HDV ribozyme-like secondary structure containing P1−P4 pairings and a weakened P1.1 comprised of just one Watson−Crick (GC) base pair (Figure 1A,B) (*14*). The minimum 68-nucleotide sequence required for self-cleavage activity was found to be highly conserved among other mammalian species. More recently, HDV-like ribozymes have been identified in diverse organisms, including insects, plants, and fish, and shown to possess self-cleavage activity in vivo (*16*).

As seen for other small ribozymes, self-cleavage of the human *CPEB3* ribozyme results in reaction products with 2′,3′-cyclic phosphate and 5′-OH termini; however, the observed first-order rate constant was determined to be only 0.01 min^{-1} ($t_{1/2}$ ~ 1 h) (*14*). This ribozyme resides in an intronic region of the *CPEB3* gene and is ~11.5 kb from the next exon. The transcribing RNA polymerase would thus take ~10 min to move from the ribozyme to the intron−3′-exon junction (*17*). Ribozyme cleavage is predicted to interfere with normal splicing of the intron. It therefore has been postulated that the slow cleavage rate observed for the human ribozyme has been selected to allow normal splicing to occur most of the time, i.e., prior to ribozyme cleavage (*14*). However, ESTs corresponding to the ribozyme sequence are readily detected, suggesting that the human ribozyme is quite active in vivo. In fact, ribozyme processing efficiencies approaching 50% are observed in brain tissue according to reverse transcriptase polymerase chain reaction (RT-PCR) analysis (*14*). It is thus possible that cellular factors such as RNA binding proteins or chaperones may increase *CPEB3* ribozyme activity in vivo.

Our earlier studies of HDV ribozyme function revealed that folding of precleaved RNA, henceforth termed precursor RNA, into a native conformation is affected by flanking sequences, alternative secondary structures, and assay conditions (*18*−*21*). Since the *CPEB3* ribozyme has been proposed to be structurally related to HDV, we decided to test the importance of these factors for self-cleavage activity. Our results indicate that the

[†]This work was supported by National Institutes of Health Grant R01-58709 to P.C.B.

*To whom correspondence should be addressed. Telephone: (814) 863-3812. Fax: (814) 865-2927. E-mail: pcb5@psu.edu.

[1]Abbreviations: HDV, hepatitis delta virus; *CPEB3*, cytoplasmic polyadenylation element-binding protein 3; EST, expressed sequence tag; ILM, iterated loop matching.

© 2010 American Chemical Society

Published on Web 06/04/2010

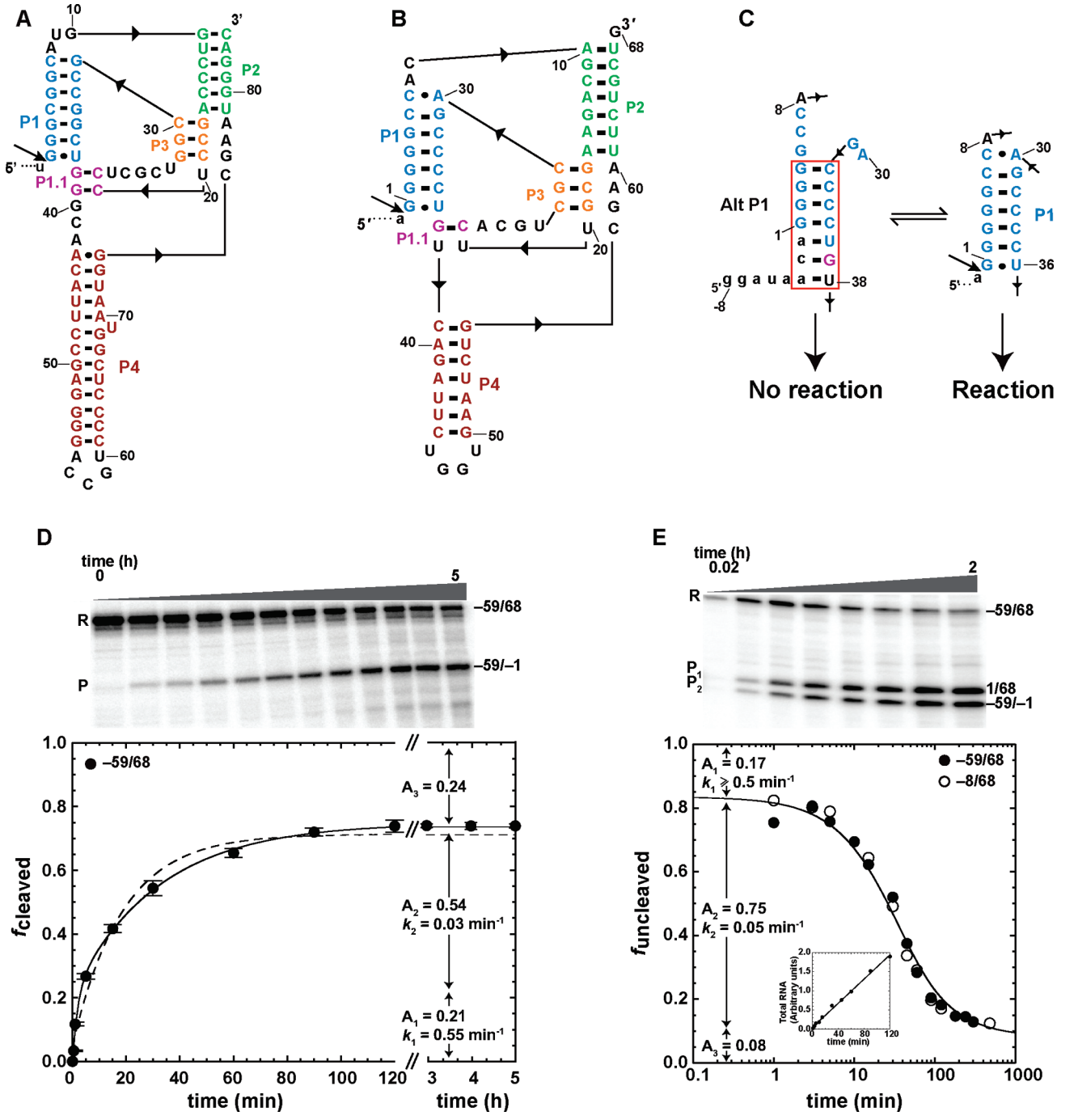

FIGURE 1: Self-cleavage of the wild-type (WT) human *CPEB3* ribozyme. (A) Secondary structure of the HDV ribozyme (*40*). (B) Secondary structure of the *CPEB3* ribozyme (*14*). (C) Equilibrium between Alt P1 and P1 for *CPEB3* ribozyme. See Figure S3 of the Supporting Information for details. (D) Denaturing 10% PAGE and kinetic traces for standard self-cleavage reactions initiated by addition of 10 mM $MgCl_2$. RNA was 5′-end-labeled with [γ-^{32}P]GTP during transcription. Also shown are plots of $f_{cleaved}$ vs time. Each data point is the average of at least two trials ± the standard error of the experiments. Data were well fit to double-exponential eq 2 (solid line, R^2 = 0.999). Poor fitting to single-exponential eq 1 is provided for comparison (dashed line, R^2 = 0.993). (E) Denaturing 10% PAGE and kinetic traces for cotranscriptional self-cleavage reactions. RNA was body-labeled with [α-^{32}P]GTP during transcription. Also shown are plots of $f_{uncleaved}$ vs time, where $R/(R + P_1 + P_2)$ represents the uncleaved fraction. Each data point is the average of at least two trials. Data for both −59/68 (●) and −8/68 (○) were fit separately to eq 3. In the shown fit, which is for −59/68, A in eq 3 was fixed at 0.08 ± 0.007, as ascertained from plateau values from gels (average ± standard deviation) averaged across 2−8 h time points for both constructs. The inset shows that the rate of transcription was constant throughout the reaction, as demanded by eq 3. 'R' is precursor, 'P' is 5′-labeled −59/−1 product. P_1 is body labeled 1/68. P_2 is body labeled −59/−1.

flanking sequence regulates self-cleavage and that the human *CPEB3* ribozyme is itself intrinsically fast-reacting.

MATERIALS AND METHODS

Cloning and Vectors. The human wild-type (WT) *CPEB3* ribozyme is located in intron 2 of the *CPEB3* gene on human chromosome 10 (NCBI accession number NC_000010). The WT plasmid containing the ribozyme sequence and 59 (or 8) upstream nucleotides was prepared by overlap extension and cloned into pUC19 downstream of a phage T7 promoter. Mutant A30G and C−2A plasmids were generated from the WT plasmid using the QuikChange kit (Stratagene). Sequences were confirmed by the dideoxy method after both miniprep and maxiprep purification (Qiagen), to control for revertants.

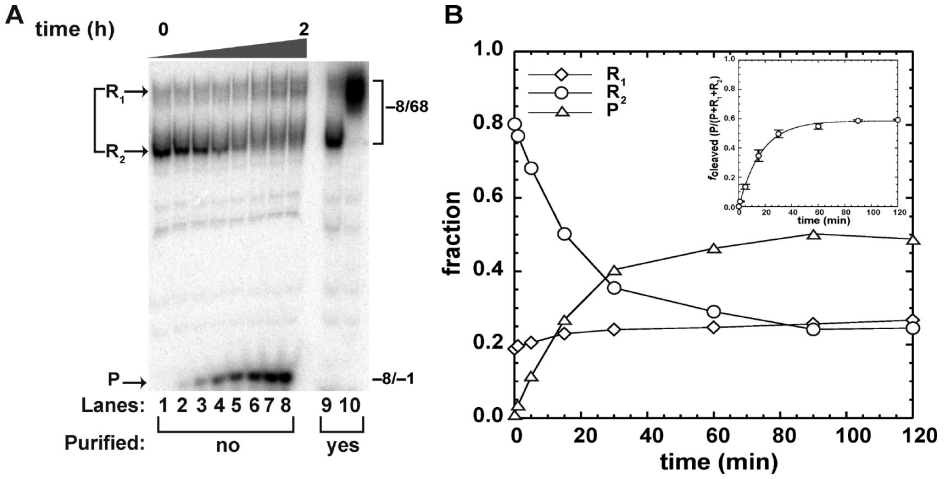

FIGURE 2: Self-cleavage of the WT human *CPEB3* ribozyme analyzed on a native gel. (A) Self-cleavage reaction of −8/68 fractionated on a 10% native gel (lanes 1−8). RNA was 5′-end labeled with [γ-^{32}P]GTP during transcription, purified, and reactions were initiated by addition of 10 mM $MgCl_2$. Full-length RNA partitions into precursor R_1 and R_2 bands and, upon self-cleavage, a −8/−1 product, P. Marker bands corresponding to native and non-native RNAs that were previously purified on a qualitative native gel, renatured at 50 °C, and fractionated on this native gel are shown in lanes 9 and 10, respectively. (B) Time-dependent change in the three RNA species fractionated on native gels. The inset is a plot of $f_{cleaved}$ vs time for the data in panel A, where $P/(R_1 + R_2 + P)$ represents the cleaved fraction. Each data point is the average of at least two trials ± the standard error of the experiments. Data were fit to eq 1.

Standard Self-Cleavage Assays Using Full-Length Transcripts. Several early attempts were made to transcribe and purify full-length RNA, followed by dephosphorylation and 5′-end labeling ("two-step purification"). However, each of these steps, which require Mg^{2+} solutions, led to extensive self-cleavage, resulting in final uncleaved RNA yields of ≤20%. Moreover, as described here, it was likely that the fastest-reacting RNAs were being lost. To improve yields, RNA transcription reactions were conducted at room temperature (22 °C) rather than the typical 37 °C, and for shorter times (2 h) rather than the typical 4 h. In addition, we eliminated the dephosphorylation and end labeling steps by conducting the transcription reaction in the presence of [γ-^{32}P]GTP (to allow 5′-end labeling) as described below, which afforded 5′-end-labeled RNA ("one-step purification").

The BsaI-digested linearized plasmid was subjected to runoff transcription (Ambion) in the presence of 30 μCi of [γ-^{32}P]GTP (to allow end labeling). Typically, a 20 μL transcription reaction was performed using 2 μg of DNA template, and the mixture was incubated at room temperature for 2 h to minimize self-cleavage. The reaction was terminated by addition of 0.1 M EDTA/95% (v/v) formamide loading buffer and the mixture fractionated on a 6% denaturing PAGE gel, run at 25 W for ∼1 h. RNA was visualized by UV shadowing, and the uncleaved full-length RNA band was excised, eluted into TEN_{250}, and precipitated with ethanol. Prior to each reaction, this 5′-end-labeled RNA was renatured at 85 °C for 5 min in 0.5 mM Tris (pH 7.5) and 0.05 mM EDTA, followed by incubation at room temperature for 10 min. Reactions were performed as previously described (*18*, *22*). A typical self-cleavage reaction mixture contained ∼2 nM 5′-end-labeled RNA, 25 mM HEPES (pH 8.0), 100 mM KCl, and 10 mM $MgCl_2$ (Figures 1D and 4A). The mixture was incubated at 37 °C for 2 min without $MgCl_2$; a zero time-point sample was removed, and self-cleavage was initiated by addition of $MgCl_2$ to a final concentration of 10 mM. Aliquots (4 μL) were withdrawn at specific time intervals, and the reactions were quenched via addition of 4 μL of 95% formamide loading buffer with 0.1 M EDTA. For most reactions, time points ranged from 1 min to 2 h. Quenched samples were fractionated on denaturing 6% PAGE gels, dried, and quantified with a PhoshorImager (Molecular Dynamics).

Cotranscriptional Self-Cleavage Assays. Plasmids were linearized with BsaI for runoff transcriptions. The linearized plasmid was treated as described previously (*18*, *21*, *23*) and resuspended in 1× TE at an approximate concentration of 1 μg/μL. Typical cotranscriptional cleavage assays were performed using 1 μL of linearized plasmid, NTPs (600 μM each), 0.5 μL of 10 μCi/μL [α-^{32}P]GTP (to allow body labeling), 20 mM Tris-HCl (pH 8.0), 100 mM KCl, 10 mM $MgCl_2$, 1 mM DTT, and 100 μg/mL acetylated bovine serum albumin (BSA) in a total reaction volume of 50 μL (Figures 1E and 4B). In some cases where lower rates of transcription were desired, 100 μM ATP, CTP, and UTP were used, and the concentration of GTP was held at 600 μM to help initiate transcription (Figure S2 of the Supporting Information). The reaction mixture was incubated for 2 min at 37 °C, followed by initiation with T7 RNA polymerase to a final concentration of 4%. Aliquots (3 μL) were withdrawn at specific times and the reactions quenched by addition to 3 μL of the 95% formamide loading buffer with 0.1 M EDTA. For most reactions, the time points ranged from 1 min to 2 h. The rate of transcription was constant over the time course of the entire experiment, as confirmed by plotting RNA concentration versus time (Figure 1E, inset), which enables fitting to standard cotranscriptional cleavage equations (see below). RNA was fractionated on 10% denaturing PAGE gels, run at 25 W for ∼1 h. Gels were dried and quantified with a PhosphorImager (Molecular Dynamics).

Native Gel Electrophoresis. Transcription reactions were conducted in the presence of [γ-^{32}P]GTP as described above to generate 5′-end-labeled precursor RNA. This RNA was subsequently used in self-cleavage reactions and fractionated on denaturing (see above) or native gels (described here). Sample aliquots (4 μL) from the self-cleavage reaction mixtures were withdrawn at specific times; the reactions were quenched by addition of 50 mM EDTA, and the solutions were mixed with 8% glycerol. Samples were loaded on a running 10% native gel that was prerun at 300 V for ∼40 min at 16 °C in 0.5× TBE (Figure 2A). A dye solution containing 20% glycerol was loaded in the outer lanes adjacent to the sample lanes to monitor the progress of the gel. The run was terminated when the lower bromophenol blue dye reached the bottom of the gel (∼3 h).

The gel was dried and quantified with a PhosphorImager (Molecular Dynamics).

Enzymatic Structure Mapping of RNA. Structure mapping experiments were conducted using 5′-end-labeled precursor or cleaved RNA (~2 nM) and RNase T1, RNase A, or RNase V1. After the self-cleavage reaction had been allowed to proceed to completion, the cleaved ribozyme was purified and 5′-end labeled. To generate precursor RNA, full-length −8/68 RNA was fractionated on a preparative gel that showed the RNA running as two diffuse bands corresponding to R_1 and R_2 (Figure 2A). These bands were purified and then 5′-end labeled prior to being used in the structure mapping experiments. A small fraction of this RNA was observed to cleave during the mapping procedure as evidenced by the dark band below G1 (Figure 3B). RNase stocks were obtained from Ambion and diluted with 50% (v/v) glycerol. Concentrations of the various RNases were as follows: RNase T1, 10^{-1}, 10^{-2}, and 10^{-3} unit/μL; RNase A, 1, 10^{-1}, and 10^{-2} ng/mL; and RNase V1, 5×10^{-3}, 5×10^{-4}, and 5×10^{-5} unit/μL. Prior to mapping, the RNA was renatured in 0.5 mM Tris, 0.05 mM EDTA, 100 mM KCl, and 10 mM $MgCl_2$ at 55 °C for 5 min and kept at room temperature for 10 min. After addition of RNases, reaction mixtures were incubated at 37 °C for 15 min, followed by addition of 95% formamide loading buffer with 100 mM EDTA, and immediately frozen in dry ice. Sequencing lanes for G were prepared by limited digestion with RNase T1 (1 unit/μL) under denaturing conditions and incubated at 50 °C for 15 min. The alkaline hydrolysis ladder was prepared by heating the RNA in a hydrolysis buffer [50 mM Na_2CO_3/$NaHCO_3$ (pH 9.0) and 1 mM EDTA] at 90 °C for 5 min. Prior to electrophoresis, samples were thawed at room temperature, boiled for 2 min, and immediately fractionated on an 8.3 M urea/12% PAGE gel.

Data Fitting. In standard assays, since the precursor RNA is 5′-end labeled, only two bands are visualized: precursor starting material (−59/68 or −8/68) and the upstream cleavage fragment (−59/−1 or −8/−1) (e.g., Figure 1D). In these assays, plots of fraction product versus time were fit to either a single exponential (eq 1) or a double exponential (eq 2). Equation 1 is as follows

$$f_c = A + Be^{-k_{obs}t} \quad (1)$$

where f_c is the fraction of precursor ribozyme cleaved, k_{obs} is the observed first-order rate constant for ribozyme cleavage for the nonburst phase, t is time, A is the fraction of ribozyme cleaved at completion, $-B$ is the amplitude of the observable phase, $1 - A$ is the unreactive fraction, and $A + B$ is the burst fraction.

Equation 2 is as follows

$$f_c = A + Be^{-k_1 t} + Ce^{-k_2 t} \quad (2)$$

where f_c is the fraction of precursor ribozyme cleaved, k_1 and k_2 are the observed first-order rate constants for the fast and slow phases, respectively, t is time, A is the fraction of ribozyme cleaved at completion, $-B$ and $-C$ are the amplitudes of the observable phases, $1 - A$ is the unreactive fraction, and $A + B + C$ is the burst fraction. For example, in Figure 1D, amplitudes A_1, A_2, and A_3 correspond to $-B$, $-C$, and $1 - A$, respectively. Each data point was the average of at least two trials ± the standard error of the experiments, and fits were weighted to the standard errors.

In cotranscriptional assays, each transcript was labeled internally as it was transcribed, allowing three bands to be visualized: precursor starting material (−59/68 or −8/68), upstream cleavage fragment (−59/−1 or −8/−1), and downstream cleavage fragment (1/68) (e.g., Figure 1E). Since reactions were initiated by addition of T7 RNA polymerase; accurate and reproducible data could only be obtained 1 min after time zero, and a small fraction of RNA was already cleaved. The equation used to fit cotranscriptional data is based on an expression derived for the case in which a full-length transcript is an intermediate in a two-step reaction of transcription followed by cleavage in which there is no burst fraction and all the RNA reacts (*24*). Since kinetic profiles for all the RNAs used in this study exhibited clear burst and nonreactive fractions, the data were fit to the following adjusted equation

$$f_{un} = A + B\left(\frac{1 - e^{-k_{obs}t}}{k_{obs}t}\right) \quad (3)$$

where f_{un} is the fraction of precursor ribozyme remaining uncleaved, k_{obs} is the observed first-order rate constant for ribozyme cleavage for the nonburst phase, t is time, A is the fraction uncleaved at completion, B is the amplitude of the observable phase, and $1 - (A + B)$ is the burst fraction. For example, in Figure 1E, amplitudes A_1, A_2, and A_3 correspond to $1 - (A + B)$, B, and A, respectively. In eq 3, the data were better fit when the value for A was constrained to the actual value obtained from the raw experimental data. We also monitored the rate of transcription and found it to be constant (Figure 1E, inset), as demanded by this model. Each data point is the average of at least two trials. We note that standard assay data are plotted with $f_{cleaved}$ on the y-axis, while cotranscriptional data are plotted as $f_{uncleaved}$: this is done because it is simpler to derive the cotranscriptional data in this fashion, and it also customary to plot cotranscriptional data this way (*18*, *24*, *25*).

All kinetic parameters were obtained using nonlinear least-squares fitting by Kaleidagraph (Synergy Software).

RESULTS

Effects of Flanking Sequence and Cotranscriptional Folding on Cleavage Rate. The kinetic properties of a 209-nucleotide version of the human *CPEB3* ribozyme, −89/68/52,[2] have been previously reported (*14*). Under standard assay conditions of Mg^{2+} initiation of self-cleavage, this construct displayed a slow rate of self-cleavage of ~0.01 min^{-1} ($t_{1/2} \sim 1$ h). These investigators also conducted kinetics experiments on a longer ribozyme construct (~−250/68/~250), which gave similar rates, indicating that further lengthening of flanking sequence has little effect on rate. We noted that this rate of cleavage is nearly 300-fold slower than previously reported values for the WT HDV genomic ribozyme under similar standard assay conditions and Mg^{2+} concentrations (*18*), and more than 6000-fold slower than those of the fastest-reacting (G11C/U27Δ) constructs from our laboratory (*20*). These observations suggested that the *CPEB3* self-cleavage reaction may be inhibited in some fashion.

Rates of HDV ribozyme reactions can be affected by four factors: (1) purification procedures, (2) length and sequence of the RNA flanking the ribozyme, (3) whether cleavage is monitored cotranscriptionally or initiated by addition of a critical reaction component, and (4) sequence of both the ribozyme and its flanking

[2]We abbreviate the constructs from Salehi-Ashtiani and co-workers as $-a/68/b$, where a is the number of nucleotides upstream of the cleavage site, b is the number of nucleotides downstream of the 3′-end of the ribozyme, and 68 is the length of the ribozyme. We use the notation $-a/68$ for our constructs because they terminate at the 3′-end of the ribozyme. Cleaved constructs are noted as 1/68.

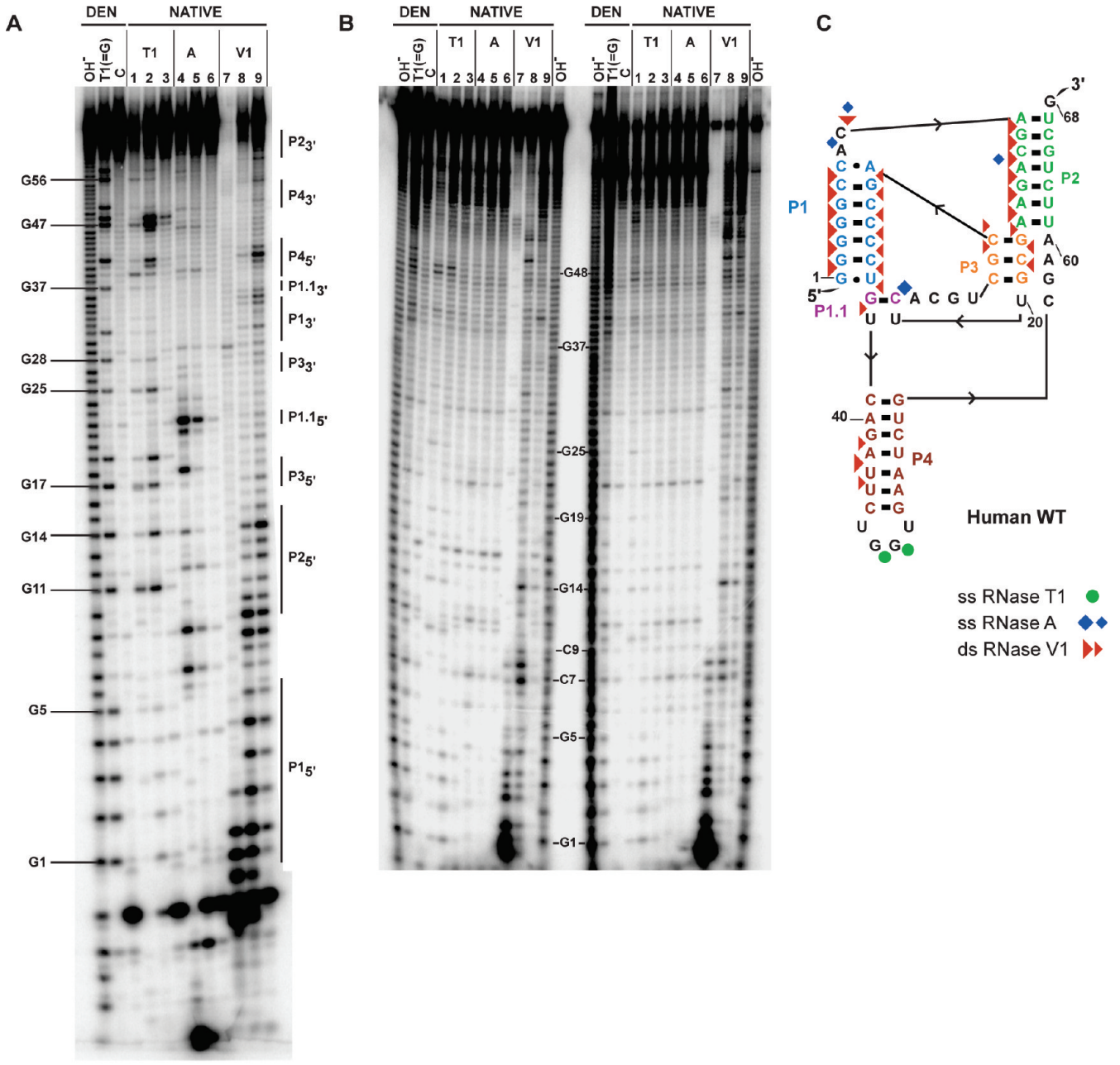

FIGURE 3: Enzymatic structure mapping of the WT human *CPEB3* ribozyme. (A) Structure mapping of the self-cleaved WT 1/68 ribozyme. A denaturing 12% polyacrylamide gel is shown. The 5′-end-labeled RNA was treated with RNases as described in Materials and Methods. The first three lanes are denaturing conditions (DEN), and the others are native conditions (NATIVE). Labels are as follows: OH^-, limited alkaline digest; T1, A, and V1, limited digests with RNases T1 (G-specific), A (pyrimidine-specific), and V1 (double-strand-specific), respectively; C, control sample without enzyme. Sets of three decreasing concentrations of each ribonuclease are provided (see Materials and Methods for details), and those with single-hit kinetics were used for structure assignments, which is the third lane in each set. The numbering to the left of the gel refers to selected bands produced by limited digestion with RNase T1. For the self-cleaved ribozyme, positions of the pairing elements are delineated by vertical lines and labeled on the right-hand side. Note that RNase V1 cleavage products greater than ~10 nucleotides in length migrate approximately 1 nucleotide slower than other cleavages because of the absence of a 2′,3′-cyclic phosphate. Fragments shorter than 10 nucleotides generated by RNase V1 cleavages have anomalous migrations relative to RNase T1 and hydrolysis lanes (*41*). There are additional bands at the very bottom of the gel that did not align with the T1 ladder and likely represent 2′- and/or 3′-phosphate monoesters. (B) Structure mapping of the precursor WT −8/68 ribozyme. The gel is labeled as described above for the cleaved ribozyme. Selected bands produced by limited digestion with RNase T1 are numbered. Lanes to the left of the numbering are for precursor RNA band R_1, and those to the right are for band R_2 (see Figure 2). Both of these bands had been purified from a native gel as described in Materials and Methods. (C) Single- and double-stranded cleavages for the self-cleaved form in panel A mapped to a secondary structure. This structure is largely consistent with structure mapping of the self-cleaved form of the ribozyme and with free energy minimizations using ILM (*29*, *30*), as well as the structure proposed by Salehi-Ashtiani et al. (*14*). Positions of cleavage by RNases T1, A, and V1 are shown using green circles, blue diamonds, and red triangles, respectively. Symbol size is relative to cleavage intensity.

regions. In this section, we consider how the first three factors contribute to *CPEB3* ribozyme reactivity; the following two sections present motivating factors for making point mutations, and the last section describes their effects on reactivity.

We first investigated the effects of ribozyme purification on kinetic behavior. Full-length −59/68 precursor RNA was synthesized by standard methods via a 4 h transcription reaction at 37 °C followed by a two-step PAGE purification (one purification

Table 1: Observed Rate Constants for the Various Human *CPEB3* Ribozymes[a]

RNA	standard assays[b]			cotranscriptional assays[c]		
	k_{obs} (min^{-1})	amplitude[d] (%)	*x*-fold effect[e]	k_{obs} (min^{-1})	amplitude[d] (%)	*x*-fold effect[e]
human −59/68 (WT)	0.55 ± 0.1	21 ± 2	55	≥5.0[g]	17 ± 2	≥50
	0.03 ± 0.003	54 ± 2	3	0.05 ± 0.004	75 ± 2	5
	nr[f]	26 ± 4	−	nr[f]	8 ± 0.7	−
human −8/68 (WT)	0.33 ± 0.08	18 ± 2	33	≥5.0[g]	13 ± 2	≥50
	0.03 ± 0.005	55 ± 4	3	0.06 ± 0.004	79 ± 2	6
	nr[f]	27 ± 5	−	nr[f]	8 ± 0.3	−
human −8/68 (C−2A)	2.6 ± 0.5	16 ± 1	260	≥5.2[g]	18 ± 1	≥250
	0.53 ± 0.06	60 ± 5	53	0.49 ± 0.02	80 ± 1	49
	nr[f]	24 ± 5	−	nr[f]	2 ± 0.5	−
chimp −8/68 (WT)	2.4 ± 0.6	42 ± 3	240	≥2.2	29 ± 3	≥220
	0.44 ± 0.02	21 ± 2	44	0.72 ± 0.06	63 ± 3	72
	nr[f]	37 ± 4	−	nr[f]	8 ± 0.2	−
chimp −8/68 (C−2A)	3.2 ± 0.2	37 ± 2	320	≥8.2	34 ± 1	≥280
	0.6 ± 0.09	17 ± 1	60	1.1 ± 0.2	60 ± 1	110
	nr[f]	45 ± 2	−	nr[f]	6 ± 0.5	−
−89/68/52[h]	0.01	70	1	−	−	−
−30/99 HDV (G11C/U27Δ)[i]	63	86	6300	−	−	−

[a]Each data point is the average of at least two trials ± the standard error of the experiments. All data are for denaturing PAGE fractionation. [b]Self-cleavage reactions of full-length RNA, which were initiated by addition of $MgCl_2$, and data were fit to eq 2. All data are for singly purified, [γ-^{32}P]GTP-labeled RNA. [c]Cotranscriptional self-cleavage assays, which were fit to eq 3. [d]Amplitudes for RNA associated with each fraction. For standard assays, the amplitude of the nr phase was determined from the fits. Errors for the nr phase were calculated using the square root of the sum of the squares of the other two amplitude errors. For cotranscriptional assays, the amplitude of the nr phase was determined experimentally from the average of long (2−8 h) time points, and associated errors are the standard deviation. These experimentally determined nr values were held constant in fits. [e]*x*-fold effects are relative to 0.01 min^{-1} for the human −89/68/52 *CPEB3* ribozyme (*14*). [f]Fraction remaining unreacted at the end of the reaction. [g]This value was estimated by substituting different values for k_1 into eq 3 and finding the lowest value that still gave a good fit to the data using the amplitudes given. [h]From ref *14*. [i]From ref *20*.

of unlabeled transcript and one of 5′-end-labeled transcript) and led to a monophasic rate plot with a relatively slow rate constant of 0.03 min^{-1} and only 44% reaction (Figure S1 of the Supporting Information). Notably, this rate constant is similar to the aforementioned rate constant of 0.01 min^{-1} for −89/68/52 (*14*). This indicates that we are able to reproduce those results and that the upstream sequence between nucleotides −89 and −59 as well as the downstream sequence has an at most minor effect on rate.

We considered the possibility that a fast-reacting ribozyme population had been lost during the extensive handling, leaving behind just slow and nonreacting species. To test this possibility, we prepared the precursor RNA using shorter transcription reactions (2 h) at lower temperatures (22 °C); moreover, we performed transcriptions in the presence of [γ-^{32}P]GTP to end-label the RNA cotranscriptionally to eliminate the second PAGE purification. These changes uncovered a faster-reacting population as revealed by both standard and cotranscriptional assays. Standard cleavage assays in which the reaction was initiated by Mg^{2+} addition led to biphasic behavior, with rate constants for −59/68 of 0.55 min^{-1} (21% amplitude) and 0.03 min^{-1} (54% amplitude) (Figure 1D and Table 1). Notably, the slower rate constant is the same as for the doubly purified ribozyme (see above), while the faster rate constant is ∼50 times faster than previously reported (*14*). These data are consistent with the idea that the faster-reacting population had been lost due to the double purification procedure and suggest that the human *CPEB3* ribozyme may have an intrinsic ability to react fast. We also note that ∼25% of the ribozyme population is nonreactive during a 5 h time course.

Next we investigated whether the length of upstream flanking sequence affects the ribozyme cleavage rate. Self-cleaving ribozymes are naturally flanked by RNA sequence, which offers the potential to regulate ribozyme reactivity (*26*). Lengthening and shortening upstream RNA regions have been shown to both enhance and inhibit the reactivity of the HDV ribozyme depending on sequence (*18*). We tested the effects of the length of the upstream sequence by comparing the kinetic behavior of −59/68 and −8/68 *CPEB3* ribozymes. These two constructs reacted nearly identically to each other under all conditions tested (summarized in Table 1), indicating that the length of upstream sequence between nucleotides −59 and −8 does not affect the rate.

The third potential contributor to ribozyme cleavage rate is folding during transcription. In the cell, RNAs can fold and cleave as they are being transcribed, and in some instances, this improves the efficiency of self-cleavage (*27*). In particular, cotranscriptional folding enhances the reactivity of the genomic HDV ribozyme depending on flanking sequence and is a necessary condition for the wild-type HDV ribozyme to be fast-reacting (*18*, *21*, *23*). We therefore examined self-cleavage of the *CPEB3* ribozyme under cotranscriptional assay conditions. As with standard cleavage assays, −8/68 and −59/68 constructs reacted identically (Figure 1E and Table 1). The cotranscriptional reaction profile for the WT *CPEB3* ribozyme has a minimum of three phases: a fast phase (17%) that gave a lower limit for k_{obs} of 0.5 min^{-1}, an intermediate phase (75%) that gave an observed rate constant of 0.05 min^{-1}, and a nonreactive phase (8%) that remained unreacted between 2 and 8 h (Figure 1E). Overall, these cotranscriptional kinetic parameters are similar to the standard assay kinetic parameters in terms of number of phases, amplitudes, and rate constants, suggesting that folding during transcription does not enhance reactivity. Slowing the rate of transcription by lowering the concentration of NTPs did not enhance the rate of self-cleavage either (Figure S2 of the Supporting Information), further supporting this conclusion. The observation that cotranscriptional assays had just 8% unreacted ribozyme, as compared to ∼25% for standard assays, may reflect the loss of fast-reacting RNA species during purification for standard assays despite the simpler one-step procedure.

To summarize, standard and cotranscriptional assays revealed that ~20% of the human *CPEB3* ribozyme reacts ~50-fold faster than previously reported. This suggested the possibility that the *CPEB3* ribozyme is intrinsically fast-reacting.

Experimental Support for Conformational Heterogeneity of the Uncleaved Human CPEB3 Ribozyme. Both standard and cotranscriptional self-cleavage reactions for the *CPEB3* ribozyme revealed fast, slow, and nonreactive populations. We therefore reasoned that the various phases might represent alternatively folded RNA species. To test this, we repeated standard self-cleavage assays on −8/68 but fractionated the RNA on a native gel (Figure 2).

Prior to initiation of the reaction, two bands containing precursor RNA, termed R_1 and R_2 for the upper and lower mobility bands, respectively, were observed (Figure 2A). The precursor bands are diffuse, suggesting each may represent populations of RNAs with different but related folds (*28*). We note that these RNAs, which have identical mobilities on a denaturing gel (see starting materials in Figure 3B), do not interconvert during native purifications or when renatured at 50 °C (Figure 2A, lanes 9 and 10). As self-cleavage progresses, a product band fragment accumulates, which was accompanied by a decrease in the amount of the R_2 species but essentially no change in the amount of R_1 (Figure 2A,B).

The fraction of each RNA species on the native gel was quantified and plotted as a function of time (Figure 2B). Native gel data for R_2 were well fit to a single exponential (eq 1) to give a k_{obs} of 0.06 min^{-1} and an end point of 58% (Figure 2B, inset). The value of k_{obs} is intermediate between the slow and fast rate constants for −8/68 fractionated on a denaturing gel of 0.33 min^{-1} (18% amplitude) and 0.03 min^{-1} (55% amplitude), respectively (Table 1), and similar to their weighted average of 0.076 min^{-1}. The similarity of the k_{obs} from the native gel assay to the weighted k_{obs} from denaturing gel assay,[3] along with a similar fraction unreacted, leads to the conclusion that there are two diffuse precursor RNA populations, only one of which is reactive. The nonreacting R_1 population has a slower mobility than R_2 on the native gel (Figure 2A), suggesting that R_1 does not have a native tertiary structure.

In an effort to understand structural features of the precursor state that lend themselves to faster reactivity, we mapped the secondary structure of the precursor R_1 and R_2 forms using a set of single- and double-strand-specific ribonucleases (Figure 3B). In parallel, we mapped the secondary structure of the cleaved form of the ribozyme (Figure 3A). The single- and double-strand-specific structure mapping bands of the cleaved form of the *CPEB3* ribozyme were well-resolved by denaturing PAGE and found to be in excellent agreement with the secondary structure proposed by Salehi-Ashtiani et al. (*14*), including the one Watson−Crick base pair P1.1 (Figure 3C). These data provide strong experimental support for the idea that the *CPEB3* ribozyme has essentially the same secondary structure as the HDV ribozyme. In contrast to the cleaved form of the ribozyme, the structure mapping bands of the precursor RNA did not indicate a unique and stable secondary structure. This observation is consistent with the diffuse nature of the fast-reacting precursor population on a native gel (Figure 2A) and suggest that the precursor ribozyme may be dynamic.

[3]The inability to resolve fast- and slow-reacting phases upon fitting native gel assay data may be due to the inability of a nondenaturing gel to fully resolve reactant and product species.

Alternative Secondary Structures. Standard and cotranscriptional assays fractionated on denaturing and native gels revealed that the *CPEB3* ribozyme partitions into fast, intermediate, and nonreacting populations. We were particularly interested in the ~20% fast-reacting population and made efforts to test whether the amplitude of that phase could be enhanced.

As the −8/68 and −59/68 constructs reacted nearly identically, we reasoned that flanking sequence between nucleotides −8 and −1 may interfere with reactivity in some fashion. To test this possibility, we predicted secondary structures for the precursor (−8/68) and cleaved (1/68) human *CPEB3* ribozyme using the iterated loop matching (ILM) folding algorithm, which enables prediction of pseudoknots (*29*, *30*). The predicted secondary structure of the cleaved ribozyme contained native P1, P2, and P4 pairings and no stable mispairings (Figure S3A of the Supporting Information). Next we predicted the secondary structure of the precursor −8/68 RNA ribozyme. This analysis suggested the potential for stable misfolded helices in the precursor RNA. Notably, while the native P2 and P4 helices were still present, a very stable alternative pairing (7 bp with five GC pairs) involving upstream nucleotides and portions of P1 and $P1.1_{3'}$ was predicted (Figure S3B of the Supporting Information). This pairing is similar in position and function, although not sequence, to the Alt P1 pairing previously shown to limit reactivity of the HDV ribozyme (*19*), so the same nomenclature is used herein. Near the base of Alt P1 in −8/68 was a CG base pair that involved C−2 of the flanking sequence. In an effort to disrupt this alternative pairing, we made a C−2A change in silico. This point mutation resulted in a predicted fold once again containing native P1, P2, and P4 pairings, and no stable alternative pairings (Figure S3C of the Supporting Information).

Next, we predicted the folding of the chimp ortholog of the human *CPEB3* ribozyme. The chimp ribozyme sequence differs from the human sequence by one change, a CA to CG change at the top of P1, which is typical of most mammalian ribozymes, and has been reported to accelerate self-cleavage severalfold (*14*). The cleaved (1/68) and precursor (−8/68) WT chimp ribozyme were predicted to be similar to the that of human RNA (Figure S3D,E of the Supporting Information): both RNAs had native P2 and P4 helices, with native P1 in 1/68 and a stable Alt P1 pairing involving upstream nucleotides and portions of P1 and $P1.1_{3'}$ in −8/68. Likewise, −8/68 chimp C−2A folds were similar to human C−2A folds, containing only native pairings, with the Alt P1 pairing observed in the chimp WT being absent (Figure S3F of the Supporting Information). We note also that, unlike in the human ribozyme, the Alt P1 pairing in the −8/68 chimp ribozyme retains a native pairing at its top, suggesting that it may not behave in a manner identical to that of the human ribozyme.

Fast Rates for CPEB3 Ribozymes with Mutant Flanking Sequences. Secondary structure predictions suggested that a C−2A mutation would destabilize a misfold in −8/68 RNAs. We therefore introduced this change into both human and chimp −8/68 ribozymes and conducted standard and cotranscriptional assays to test whether this led to enhanced cleavage kinetics. Standard cleavage assays of the C−2A human ribozyme with the [γ-^{32}P]GTP-labeled ribozyme maintained biphasic behavior; however, the observed rate constants were 2.6 min^{-1} (16% amplitude) and 0.53 min^{-1} (60% amplitude). A nonreactive fraction of ~25% was also observed (Figure 4A). These amplitudes are similar to those for the WT −8/68 ribozyme, but

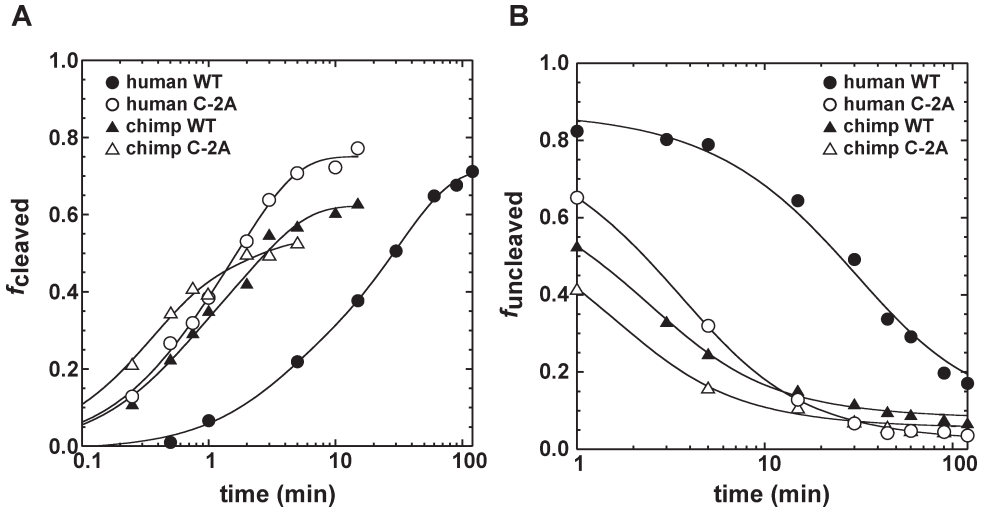

FIGURE 4: Self-cleavage of human and chimp *CPEB3* WT and C−2A ribozymes. Standard (A) and cotranscriptional (B) self-cleavage reactions for human WT (●), human C−2A (○), chimp WT (▲), and chimp C−2A (△). Initiation of the reaction, generation of plots, and fitting of data were the same as in Figure 1. Human and chimp ribozyme constructs were −8/68.

the rates of the fast and intermediate phases were increased by ~8- and ~18-fold, respectively (Table 1).

Cotranscriptional cleavage assays of the C−2A human ribozyme also revealed biphasic behavior. In this assay, the rate constant for the intermediate phases increased by ~8-fold relative to that of the WT human *CPEB3* ribozyme under cotranscriptional assay conditions (Figure 4B). As observed with the WT human ribozyme, the nonreactive phase of C−2A was much smaller in amplitude cotranscriptionally than for standard assays, further suggesting that the simpler one-step purification still loses some of the most reactive ribozymes.

Next, we investigated the kinetic behavior of the chimp *CPEB3* ribozyme, first under standard conditions (Figure 4A). In a WT background, the chimp ribozyme reacts faster than the human ribozyme, as expected (*14*). Like the human ribozyme, it has biphasic behavior, with rate constants of 2.4 min^{-1} (42% amplitude) and 0.44 min^{-1} (21% amplitude), along with a nonreactive fraction (37%). These rate constants are substantially faster (7−15-fold) than that of human WT but are quite similar to that of the human C−2A ribozyme. Moreover, the C−2A mutation in the chimp provides only ~1.3-fold increases in the fast and intermediate phases. The simplest interpretation of this behavior is that the chimp ribozyme is already biased toward the native state by the increased stability of its P1 helix. Thus, the WT chimp ribozyme reacts like the C−2A human ribozyme and benefits little itself from the C−2A change. Finally, conducting assays of the WT and C−2A chimp ribozymes cotranscriptionally gave rate constants that were largely in agreement with the results of standard assays. As observed in the human ribozyme, the nonreactive phase was much smaller in amplitude for cotranscriptional assays, again supporting the potential loss of the most active ribozymes.

DISCUSSION

Naturally occurring self-cleaving RNAs have been identified in numerous organisms, including viruses, bacteria, plants, insects, fish, and mammals (*7*, *16*, *31*−*33*). Mammalian ribozymes are a recent addition to this group and are present in various noncoding regions of genes (*13*−*15*). The WT human *CPEB3* ribozyme has been shown to adopt a complex tertiary structure resembling the well-characterized HDV ribozyme fold (*14*). Using RNA transcribed from human genomic DNA, a slow first-order observed rate constant of 0.01 min^{-1} was reported for the WT human *CPEB3* ribozyme (*14*). In contrast, fast rate constants of ~60 min^{-1} have been reported for certain homogeneously folded HDV ribozyme sequences (*20*). In general, RNA is prone to adopting alternative folds that depopulate the native fold, resulting in slower reaction rates (*34*), although these can often be eliminated by site-directed mutations (*35*).

Previous studies from our laboratory focused on defining the nature and role of misfolds in HDV ribozyme kinetics (*18*, *19*). In the course of these studies, most alternative pairings were found to inhibit reactivity, although certain alternative pairings acted as "folding guides" (*36*) to facilitate fast-folding kinetics (*20*). We also found that the WT sequence is optimally active, although only under cotranscriptional conditions (*21*). A combination of these approaches was used in this study to test whether the human *CPEB3* ribozyme reacts faster under certain assay conditions.

The kinetic profile of the human *CPEB3* ribozyme was found to be complex. The data could be best explained by three populations, with the fastest population (15−20%) reacting 33-fold faster in the WT background and ~250-fold faster in the C−2A background, as compared to −89/68/52. The faster rate is similar to those of the chimp ribozyme in both WT and C−2A backgrounds. Because the WT chimp ribozyme has a more stable P1, these observations support C−2A operating in the human ribozyme by depopulating a misfold of P1, as supported computationally. The misfold of P1 sequesters the 3′-strand of P1.1, preventing P1.1 formation (Figure 1C). Given that P1.1 in the *CPEB3* ribozyme consists of just one Watson−Crick base pair, this equilibrium is easily tilted toward the misfold. Consistent with this idea, adding a base pair back to P1.1, by a U38A mutation, was shown to increase the rate of self-cleavage by 9-fold (*14*). One possibility is that P1.1 is under selective pressure to have modest stability to be subject to greater regulation (see below).

Notably, folding during transcription enhances the fraction of reacted ribozyme, decreasing the amplitude of the nonreactive fold to ≤8% in WT and C−2A backgrounds. This probably occurs because the one-step RNA purification, despite being conducted at a lower temperature and for shorter times, still likely depletes at least some of the most active ribozymes from the

total population. In fact, it remains possible that the depleted population reacts more than 250-fold faster than −89/68/52: the human C−2A *CPEB3* ribozyme still reacts ~25-fold slower than the fastest HDV ribozyme constructs (Table 1), supporting this possibility. The fact that the experimentally determined fold of the cleaved ribozyme is essentially the same as the fold of the HDV ribozyme (Figure 3) also supports the notion of even greater intrinsic reactivity.

The reactivity of the human *CPEB3* ribozyme is significantly faster than previously reported (*14*). Moreover, the enhanced reactivity can be achieved by changing the flanking sequence only, indicating that the ribozyme itself is intrinsically fast-reacting. Certain cellular factors might enhance reactivity of the ribozyme in vivo, as suggested by the higher extent of the *CPEB3* ribozyme cleavage reported in certain tissues, such as brain (*14*). Such factors need not interact with the ribozyme itself, which is quite complex in structure; instead, they might simply sequester the upstream single-stranded RNA sequence that induces the misfold. This suggests that single-stranded RNA binding proteins such as hnRNPs, which coat transcripts and often act as nonspecific RNA chaperones by facilitating refolding events (*37*, *38*), might enhance folding of the human *CPEB3* ribozyme in vivo (*39*). By having a high intrinsic reactivity that is suppressed by the flanking sequence, the human *CPEB3* ribozyme potentially lends itself to regulation in response to environmental cues.

ACKNOWLEDGMENT

We thank Barbara Golden and Andrej Lupták for comments on the manuscript.

SUPPORTING INFORMATION AVAILABLE

Self-cleavage of "two-step-purified" WT human *CPEB3* ribozyme, noneffect of lowering the transcription rate, and predicted secondary structures for WT and mutant *CPEB3* ribozymes. This material is available free of charge via the Internet at http://pubs.acs.org.

REFERENCES

1. Symons, R. H. (1997) Plant pathogenic RNAs and RNA catalysis. *Nucleic Acids Res. 25*, 2683–2689.
2. Wu, H. N., Lin, Y. J., Lin, F. P., Makino, S., Chang, M. F., and Lai, M. M. (1989) Human hepatitis delta virus RNA subfragments contain an autocleavage activity. *Proc. Natl. Acad. Sci. U.S.A. 86*, 1831–1835.
3. Chen, J. L., and Pace, N. R. (1997) Identification of the universally conserved core of ribonuclease P RNA. *RNA 3*, 557–560.
4. Doudna, J. A., and Lorsch, J. R. (2005) Ribozyme catalysis: Not different, just worse. *Nat. Struct. Mol. Biol. 12*, 395–402.
5. Forster, A. C., and Symons, R. H. (1987) Self-cleavage of virusoid RNA is performed by the proposed 55-nucleotide active site. *Cell 50*, 9–16.
6. Kuo, M. Y., Goldberg, J., Coates, L., Mason, W., Gerin, J., and Taylor, J. (1988) Molecular cloning of hepatitis delta virus RNA from an infected woodchuck liver: Sequence, structure, and applications. *J. Virol. 62*, 1855–1861.
7. Saville, B. J., and Collins, R. A. (1990) A site-specific self-cleavage reaction performed by a novel RNA in *Neurospora* mitochondria. *Cell 61*, 685–696.
8. Butcher, S. E., and Burke, J. M. (1994) Structure-mapping of the hairpin ribozyme. Magnesium-dependent folding and evidence for tertiary interactions within the ribozyme-substrate complex. *J. Mol. Biol. 244*, 52–63.
9. Cech, T. R. (1988) Conserved sequences and structures of group I introns: Building an active site for RNA catalysis—a review. *Gene 73*, 259–271.
10. Michel, F., Umesono, K., and Ozeki, H. (1989) Comparative and functional anatomy of group II catalytic introns—a review. *Gene 82*, 5–30.
11. DePriest, P. T., and Been, M. D. (1992) Numerous group I introns with variable distributions in the ribosomal DNA of a lichen fungus. *J. Mol. Biol. 228*, 315–321.
12. Lai, M. M. (2006) Hepatitis delta antigen: biochemical properties and functional roles in HDV replication. In Hepatitis Delta Virus (Handa, H., and Yamaguchi, Y., Eds.) pp 38−51, Landes Bioscience, Georgetown, TX.
13. Martick, M., Horan, L. H., Noller, H. F., and Scott, W. G. (2008) A discontinuous hammerhead ribozyme embedded in a mammalian messenger RNA. *Nature 454*, 899–902.
14. Salehi-Ashtiani, K., Luptak, A., Litovchick, A., and Szostak, J. W. (2006) A genomewide search for ribozymes reveals an HDV-like sequence in the human CPEB3 gene. *Science 313*, 1788–1792.
15. Luptak, A., and Szostak, J. W. (2008) Mammalian Self-Cleaving Ribozymes, Royal Society of Chemistry, Cambridge, U.K.
16. Webb, C.-H. T., Riccitelli, N. J., Ruminski, D. J., and Lupták, A. (2009) Widespread occurrence of self-cleaving ribozymes. *Science 326*, 953.
17. Ucker, D. S., and Yamamoto, K. R. (1984) Early events in the stimulation of mammary tumor virus RNA synthesis by glucocorticoids. Novel assays of transcription rates. *J. Biol. Chem. 259*, 7416–7420.
18. Chadalavada, D. M., Knudsen, S. M., Nakano, S., and Bevilacqua, P. C. (2000) A role for upstream RNA structure in facilitating the catalytic fold of the genomic hepatitis delta virus ribozyme. *J. Mol. Biol. 301*, 349–367.
19. Chadalavada, D. M., Senchak, S. E., and Bevilacqua, P. C. (2002) The folding pathway of the genomic hepatitis delta virus ribozyme is dominated by slow folding of the pseudoknots. *J. Mol. Biol. 317*, 559–575.
20. Brown, T. S., Chadalavada, D. M., and Bevilacqua, P. C. (2004) Design of a highly reactive HDV ribozyme sequence uncovers facilitation of RNA folding by alternative pairings and physiological ionic strength. *J. Mol. Biol. 341*, 695–712.
21. Chadalavada, D. M., Cerrone-Szakal, A. L., and Bevilacqua, P. C. (2007) Wild-type is the optimal sequence of the HDV ribozyme under cotranscriptional conditions. *RNA 13*, 2189–2201.
22. Nakano, S., Chadalavada, D. M., and Bevilacqua, P. C. (2000) General acid-base catalysis in the mechanism of a hepatitis delta virus ribozyme. *Science 287*, 1493–1497.
23. Diegelman-Parente, A., and Bevilacqua, P. C. (2002) A mechanistic framework for co-transcriptional folding of the HDV genomic ribozyme in the presence of downstream sequence. *J. Mol. Biol. 324*, 1–16.
24. Long, D. M., and Uhlenbeck, O. C. (1994) Kinetic characterization of intramolecular and intermolecular hammerhead RNAs with stem II deletions. *Proc. Natl. Acad. Sci. U.S.A. 91*, 6977–6981.
25. Pan, T., Artsimovitch, I., Fang, X. W., Landick, R., and Sosnick, T. R. (1999) Folding of a large ribozyme during transcription and the effect of the elongation factor NusA. *Proc. Natl. Acad. Sci. U.S.A. 96*, 9545–9550.
26. Cao, Y., and Woodson, S. A. (1998) Destabilizing effect of an rRNA stem-loop on an attenuator hairpin in the 5′ exon of the *Tetrahymena* pre-rRNA. *RNA 4*, 901–914.
27. Pan, T., and Sosnick, T. (2006) RNA folding during transcription. *Annu. Rev. Biophys. Biomol. Struct. 35*, 161–175.
28. Koculi, E., Hyeon, C., Thirumalai, D., and Woodson, S. A. (2007) Charge density of divalent metal cations determines RNA stability. *J. Am. Chem. Soc. 129*, 2676–2682.
29. Ruan, J., Stormo, G. D., and Zhang, W. (2004) An iterated loop matching approach to the prediction of RNA secondary structures with pseudoknots. *Bioinformatics 20*, 58–66.
30. Ruan, J., Stormo, G. D., and Zhang, W. (2004) ILM: A web server for predicting RNA secondary structures with pseudoknots. *Nucleic Acids Res. 32*, W146–W149.
31. Forster, A. C., and Symons, R. H. (1987) Self-cleavage of plus and minus RNAs of a virusoid and a structural model for the active sites. *Cell 49*, 211–220.
32. Buzayan, J. M., Gerlach, W. L., and Bruening, G. (1986) Satellite tobacco ringspot virus RNA: A subset of the RNA sequence is sufficient for autolytic processing. *Proc. Natl. Acad. Sci. U.S.A. 83*, 8859–8862.
33. Sharmeen, L., Kuo, M. Y., Dinter-Gottlieb, G., and Taylor, J. (1988) Antigenomic RNA of human hepatitis delta virus can undergo self-cleavage. *J. Virol. 62*, 2674–2679.
34. Treiber, D. K., and Williamson, J. R. (1999) Exposing the kinetic traps in RNA folding. *Curr. Opin. Struct. Biol. 9*, 339–345.
35. Treiber, D. K., and Williamson, J. R. (2001) Beyond kinetic traps in RNA folding. *Curr. Opin. Struct. Biol. 11*, 309–314.

36. Isambert, H., and Siggia, E. D. (2000) Modeling RNA folding paths with pseudoknots: Application to hepatitis delta virus ribozyme. *Proc. Natl. Acad. Sci. U.S.A. 97*, 6515–6520.
37. Herschlag, D. (1995) RNA chaperones and the RNA folding problem. *J. Biol. Chem. 270*, 20871–20874.
38. Russell, R. (2008) RNA misfolding and the action of chaperones. *Front. Biosci. 13*, 1–20.
39. Mahen, E. M., Watson, P. Y., Cottrell, J. W., and Fedor, M. J. (2010) mRNA secondary structures fold sequentially but exchange rapidly in vivo. *PLoS Biol. 8*, e1000307.
40. Ferre-D'Amare, A. R., Zhou, K., and Doudna, J. A. (1998) Crystal structure of a hepatitis delta virus ribozyme. *Nature 395*, 567–574.
41. Brown, T. S., and Bevilacqua, P. C. (2005) Method for assigning double-stranded RNA structures. *BioTechniques 38*, 368, 370, 372.